Induction motor drive based on modular-multilevel converter with ripple-power decoupling channels

Enaam Abdul-Khaliq Ali[1], Turki Kahawish Hassan[2]

[1]Department of Electrical Engineering, College of Engineering, Baghdad University, Baghdad, Iraq
[2]Department of Electrical Engineering, College of Engineering, Mustansiriyah University, Baghdad, Iraq

Article Info

ABSTRACT

A driving system for a three-phase variable-speed induction machine-based modular multilevel converter (MMC) with magnetic channels operating at high frequencies-connecting adjacent-arm submodules is displayed in this paper. The primary disadvantage of using MMC in variable-speed motors is a high voltage ripple generated by submodule capacitors at low speeds with constant torque. This study utilizes the dual half-bridge (DHB) modules as energy channels, exchanging between the submodule (SM) capacitors to correct the power imbalance. The ripple power of adjacent-arm SMs may be entirely decoupled, outcomes a virtually fluctuation-set free SM capacitor voltage design. Thus, the typical MMC issue of significant ripple voltage between SM capacitors has been wholly addressed regardless of operating frequency. The design and analysis of field-oriented control (FOC) of induction motors is based on an algorithm that ensures the motor's efficiency across a broad speed range. In this paper, we achieved a tiny ripple in the capacitive voltage for some frequencies (50 Hz, 25 Hz, 10 Hz, and 5 Hz) by (±0.25%) compared with the previous papers that achieved a reduction in ripple within (±5%), and also this system was compared with the traditional system method operating principle was presented analytically and verified using MATLAB/Simulink.

Corresponding Author:

Enaam Abdul-Khaliq Ali
Department of Electrical Engineering, College of Engineering, Baghdad University
Baghdad, Iraq
Email: enaamalimsc2009@yahoo.com

1. INTRODUCTION

Modular multilevel converters (MMC) are attracting significant interest in many fields of high-power applications due to their scalability, flexibility, and controllability. Examples include high voltage direct current transmission (HVDC), high voltage DC/DC transformers, grid-connected inverters, and medium voltage motor drives (MVMD) [1]-[11]. The primary issue with traditional MMC for variable speed drives is the high sub-module fluctuation in capacitor voltage, particularly at lower speeds. The peak-to-peak capacitor voltage ripple is proportional to the load current amplitude and inversely proportional to the supply frequency. The high voltage ripple raises the switches' voltage rating [12]-[15]. Several solutions for dealing with capacitive voltage ripple of SM in variable speed drive systems have been presented in various researches. At present, the commonly used method of suppressing capacitor voltage fluctuation is to insert high-frequency common-mode voltage and bridge arm circulating current into the MMC [16]. Still, the insertion of common-mode voltage will cause damage to the motor. The damage to the edge and the bearing and the injected high-frequency circulating current will increase the capacity and loss of the converter. SM condenser voltage-ripple suppression from many viewpoints was studied [17]. The control methods adopted to develop the SM capacitor

voltage-ripple profile, a hybrid MMC architecture that integrates a conventional MMC with a DC-link sequence switch. Consequently, a ripple in capacitor voltage is reduced, especially at low motor speeds. Several changes to the fundamental MMC structure have been proposed to solve the power imbalance issue between the MMC arms. A back-to-back MMC to reduce voltage ripple in the capacitor, the grid-side MMC produces a current source at its output instead of a DC voltage source. A three-phase induction motor is driven using this current source to input the motor-side MMC. Due to the current source, the voltage-ripple of the SM capacitor is seen to remain constant until shallow frequency [13]-[19]. Also, other researchers suggested a back-back hybrid MMC that is applied to four-quadrant motor drive applications, retaining the benefits of hybrid MMC in terms of decreased capacitor voltage ripple at zero motor speeds while avoiding the use of massive filters at the direct current (DC) connection [20].

This paper uses a modular multilevel converter (MMC) with high-frequency magnetic channels to link neighboring-arm submodules (SMs). The design uses dual half-bridge (DHB) chains to connect neighboring SMs of three-phase identical arms. The DHB modules act as energy conduits, allowing power interchange between SM capacitors. The bidirectional energy transmission between neighboring-arm SMs decouples the arms' ripple power, resulting in a capacitor's near-linear SM voltage profile. Thus, the MMC's frequent issue of large voltage fluctuation between significant SM capacitors is fully addressed regardless of operation frequency [21]-[23] and the induction motor can be operated at low speed and full load.

The suggested modular multilevel converter with dual half-bridge (MM-DHB), for ripple power decoupling drive system arrangement, is outlined in section 2. Algorithms for drive systems are discussed in section 3. System simulation is illustrated in section 4, and the results are obtained and discussed in section 5.

2. MMC-DHB DRIVE SYSTEM CONFIGURATION

Figure 1 shows the proposed system configuration of the MMC-DHB motor drive for a three-phase induction motor; MMC has two arms, upper and lower, linked by buffering inductors. Every component comprises N half-bridge SMs, every with a DC capacitor and two insulated gate bipolar transistors (IGBTs) [21]. Figure 2 shows the performance of the main parts of the system. Figure 2(a), shows providing the best harmonic cancellation properties where the N triangular carriers of each arm are gradually shifted by 2π /N. As a result, the phase angles θ_L (i) and θ_U (i) of the ith carrier C_{Li} and C_{Ui} in the lower and upper arms may be calculated using (1) and (2).

$$\theta_L(i) = \frac{2\pi}{N} \times (i - 1) \tag{1}$$

$$\theta_U(i) = \theta + \frac{2\pi}{N} \times (i - 1) \tag{2}$$

The angle of displacement between the upper and lower carriers is denoted as θ. It's important to note that has a considerable influence on MMC's harmonic characteristics [24]. From the equivalent circuit diagram of one phase of MMC, as illustrated in Figure 2(b), is utilized for analysis, the output voltage and current are denoted by symbols v_{oj} and i_{oj} describes as (3) and (4):

$$v_{o_j} = V_o \cos(\omega t + \theta_j) \tag{3}$$

$$i_{o_j} = I_o \cos(\omega t + \theta_j - \varphi) \tag{4}$$

where j {A, B, C}, V_o and I_o are the amount of voltage and current, respectively, ω is the angular frequency of the output, θ_j is the stator voltage's phase angle (θ_A=0⁰, θ_B=120⁰, and θ_C=240⁰), and φ, where is the power factor of the load. The amount of the ac output voltage is as shown in (5) and (6):

$$V_o = \frac{1}{2} M V_{dc} \tag{5}$$

$$M = \frac{\omega_o}{\omega_{rated}} \tag{6}$$

where M denoted the modulation index, while V_{dc} input voltage source.
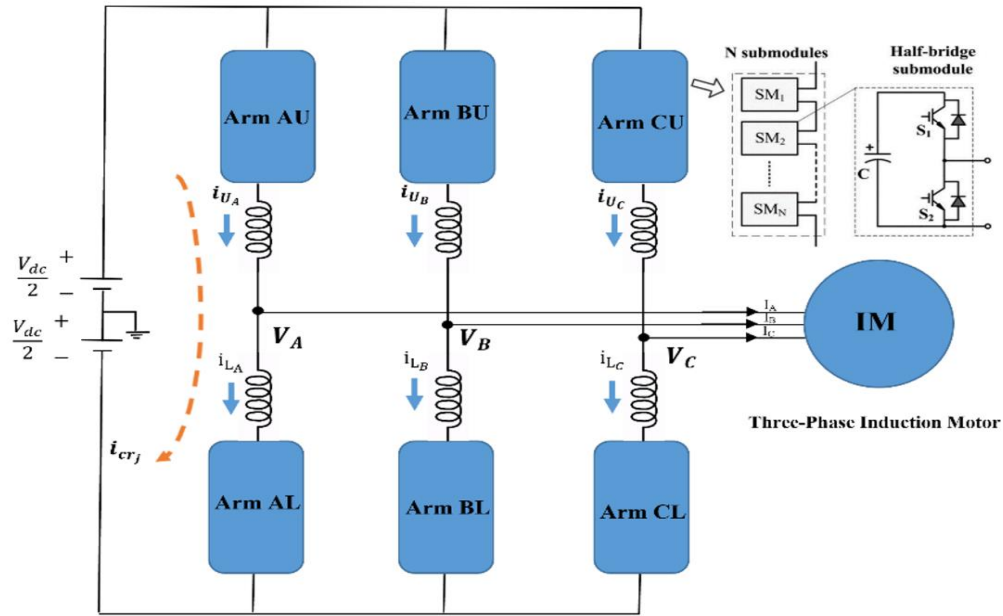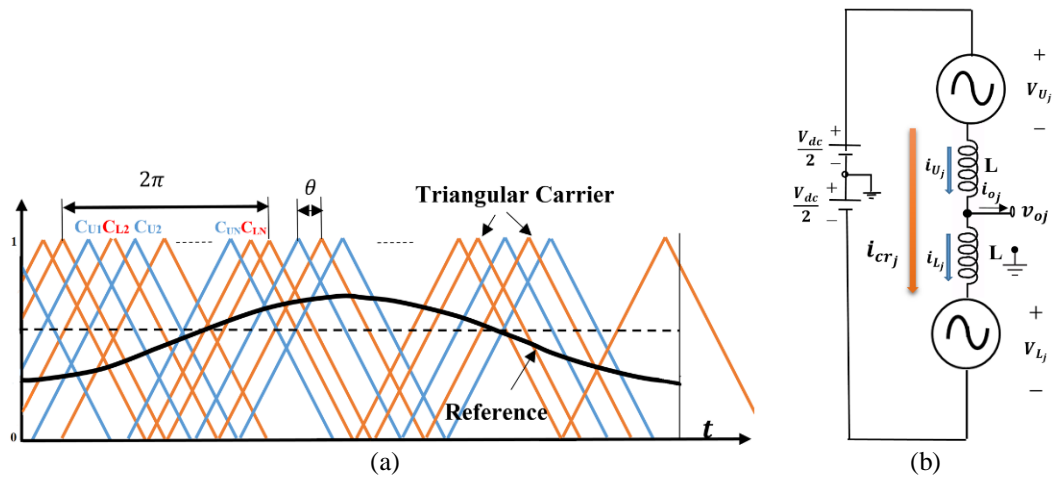
Figure 1. Drive system configuration

Figure 2. Performance of the main parts of the system (a) phase-shifted carrier (PSC) modulation and
(b) one phase equivalent circuit of MMC

The arming voltage and current of the MMC and the j-phase current (DC component current or circulating current) are described in (7)-(11) [22].

$$V_{U_j} = \frac{1}{2} V_{dc} - v_{j_o} \tag{7}$$

$$V_{L_j} = \frac{1}{2} V_{dc} + v_{j_o} \tag{8}$$

$$i_{U_j} = i_{cr_j} + \frac{1}{2} i_{o_j} \tag{9}$$

$$i_{L_j} = i_{cr_j} - \frac{1}{2} i_{o_j} \tag{10}$$

$$i_{cr_j} = \frac{i_{U_j} + i_{L_j}}{2} \tag{11}$$

The circulating current (i_{cr_j}) can be considered as a DC for even-order harmonic elimination control, which is (12).

$$i_{cr_j} = \frac{1}{3} I_{dc} = \frac{MI_o \cos\varphi}{4} \qquad (12)$$

The capacitor voltage fluctuation contains each of the CM and DM items alternating at ω_t and $2\omega_t$ because of the dual-frequency variation of the typical MMC arm energy as seen in (13) and (14) [22].

$$\Delta v_{C_{Uj}} = -\frac{\Delta V_{C_{cm}}}{2} \sin[2(\omega_t + \theta_j) - \varphi] + \frac{\Delta V_{C_{dm}}}{2} \sin(\omega_t + \theta_j - \varphi) \qquad (13)$$

$$\Delta V_{C_{Lj}} = -\frac{\Delta v_{C_{cm}}}{2} \sin[2(\omega_t + \theta_j) - \varphi] - \frac{\Delta v_{C_{dm}}}{2} \sin(\omega_t + \theta_j - \varphi) \qquad (14)$$

where Δv_C defines the capacitor voltage variation and ΔV_C defines the SM ripple's in capacitor voltage absolute peak-to-peak fluctuation, respectively. The magnitudes of the peak-to-peak capacitor voltage-ripple due to CM and DM components are shown in (15) and (16) [21]-[22].

$$\Delta V_{C_{cm}} = \frac{I_o M}{8\omega C} \qquad (15)$$

$$\Delta V_{C_{dm}} = \frac{I_o}{4\omega C} \sqrt{4 + \cos^2(\varphi)(M^4 - 4M^2)} \qquad (16)$$

The fluctuation of capacitor voltage produces by two components CM and DM. The fluctuation in capacitor voltage was very little affected by the CM component that appears only when the load current increase regardless of operating frequency, but the DM item has a significant effect on ripple which increased dramatically with reducing the frequency of operation and increasing the current output.

A proposed MMC-DHB configuration, shown in Figure 3, Allows the transfer of the ripple force from one SM with extra capacitive power stored to another SMs in a closed magnetic ring, to insufficient power supply over there, redistributes the capacitive energy that has been stored across all three SMs of the adjacent arm.
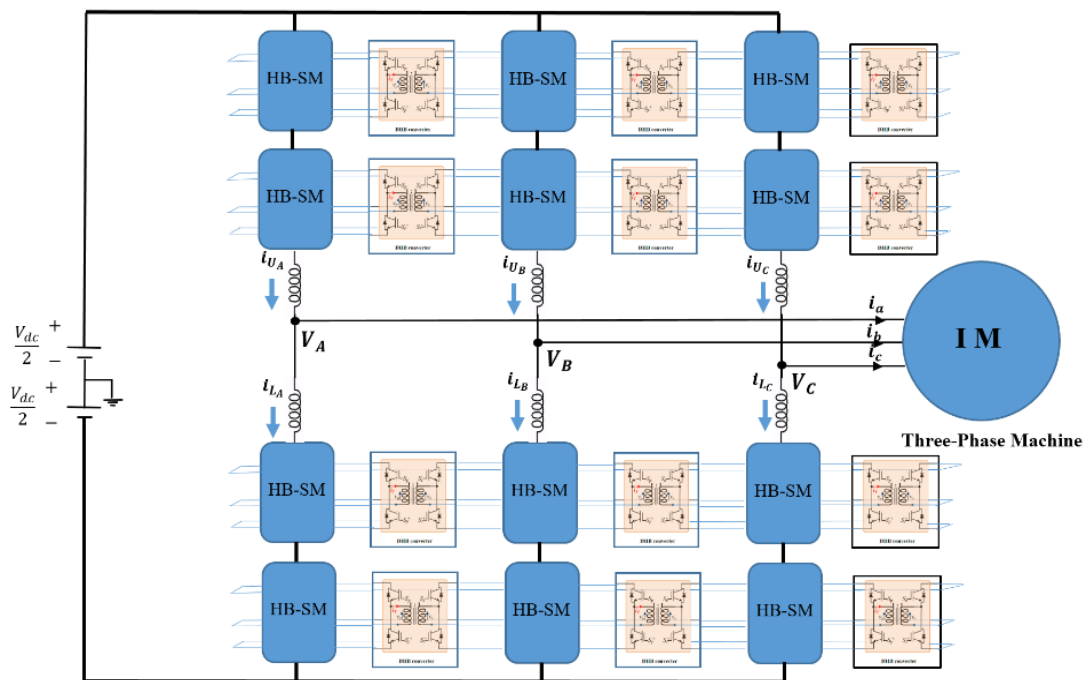

Figure 3. MMC-DHB drive system configuration [22]

3. CONTROL SYSTEM FOR MMC-DHB DRIVE IN VARIOUS SPEED

3.1. MMC Control

3.1.1. Averaging capacitor voltage control

The schematic diagram of a complete leg (phase) averaging shown in Figure 4 capacitor voltage control, consists of two loops, in the first loop the upper and lower arm's estimated capacitor voltages as illustrated in (17).

$$V_{C_{jav}} = \frac{1}{2N} \sum_{k=1}^{N} \left[V_{C_{U_{jk}}} + V_{C_{L_{jk}}} \right] \tag{17}$$

Subtracting from the reference capacitor voltage and the error handling via the proportional-integral (PI) controller to result in a reference current $i_{cr_j}^*$ the circulating current calculated in (11) is forced to follow the reference current $i_{cr_j}^*$ and fed to another PI controller in the second loop to generate an average voltage V_{dc_s} as shown in (18) and (19) [25]-[26].

$$i_{cr}^* = k_1 \left(V_C^* - V_{C_{jav}} \right) + k_2 \int \left(V_C^* - V_{C_{jav}} \right) dt \tag{18}$$

$$V_{dc_s} = k_3 \left(i_{cr_j} - i_{cr_j}^* \right) + k_4 \int \left(i_{cr_j} - i_{cr_j}^* \right) dt \tag{19}$$
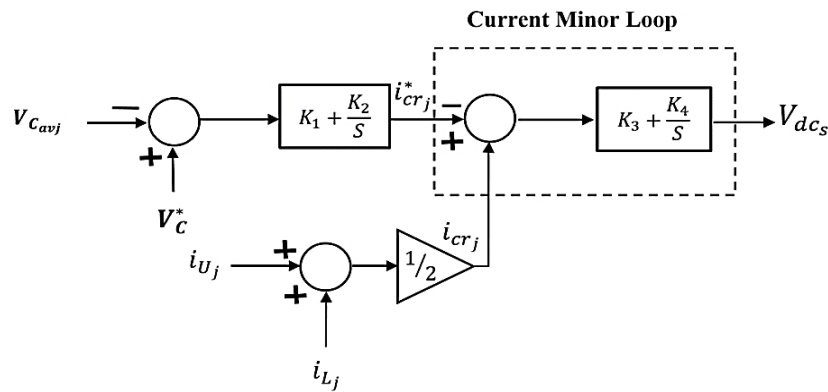

Figure 4. Schematic diagram of SM capacitor voltage averaging controller

3.1.2. Balancing controller of capacitor voltages

Arm and individual balancing capacitor control are characteristics of this kind of control. The proportional controller of gain k_5 balances the average capacitor voltages of the upper and lower arms of MMC in Figure 5 ($V_{CU_j}^{av}$ and $V_{CL_j}^{av}$) respectively as shown in Figure 5(a). A voltage reference is produced for each SM by the arm balancing controller as illustrated in (20) [12].

$$V_{j_{arm}} = k_5 \left(V_{CU_j}^{av} - V_{CL_j}^{av} \right) \tag{20}$$

The difference between each arm's average capacitor voltage ($V_{CU_j}^{av}$ or $V_{CL_j}^{av}$) and its SM capacitor voltage ($V_{C_{U_{jk}}}$ or $V_{C_{L_{jk}}}$) is used to organized the capacitor voltage of every SM of each arm. The reference signals for each upper or lower SM are obtained as shown in Figure 5(b). Proportional gains (K_6 and k_7), are used to generate extra DC voltage references for every SM, as shown in (21) and (22) [12].

$$V_{dc_{jUk}} = K_6(V_{CU_j}^{av} - V_{C_{U_{jk}}}) \tag{21}$$

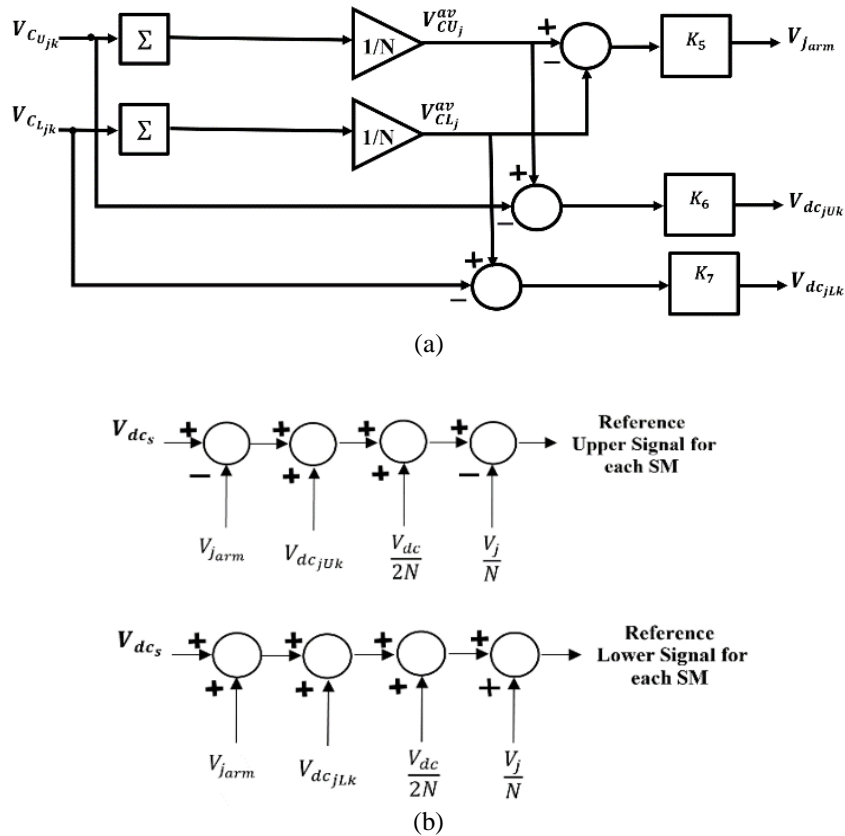$$V_{dc_{jLk}} = k_7(V_{CL_j}^{av} - V_{C_{L_{jk}}}) \tag{22}$$

(a)

(b)

Figure 5. MMC capacitor voltage balancing controllers, (a) arm and Individual SM balancing controller and (b) reference signal for each SM arm (upper and lower)

3.2. The DHB modules' control

The DHB converter is utilized as a DC-DC energy-exchange unit that achieves energy rebalancing for MMC SMs. The DHB converter is composed of a pair of voltage-fed HB inverters connected through an HF transformer. The transformer turns ratio is unity since the DC-DC conversion is only used for energy balancing between bridge sides at the same voltage level. DHB components are employed to achieve some operational characteristics, where the leakage inductance of the HF transformer is used as an energy transfer element between the DC capacitors, while the output capacitance of switching devices is used to achieve soft-switching operation. The circuit diagram for one of the magnetic chains linking adjacent-arm SMs is shown in Figure 6.
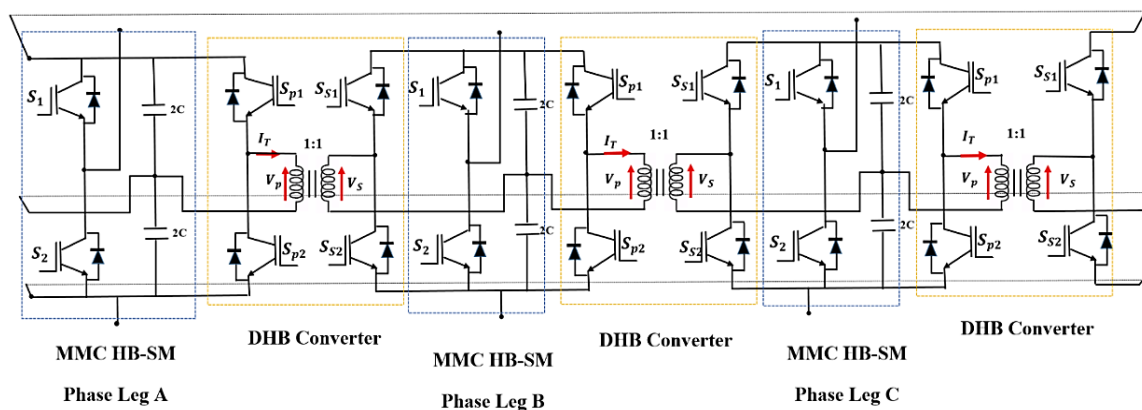

Figure 6. The circuit diagram for one of the magnetic chains linking adjacent-arm SMs [21]

Finally, the DHBs are regulated by rebalancing the stored capacitive energy between the SMs. Every DHB module contains a loop of control with a PI regulator to ensure ripple-free SM capacitor voltage. A potential difference between each pair of primary and secondary DHB capacitors is set to zero by the PI controller, which results in the desired phase angle δ* being used as an input to the DHB modulator as shown in Figure 7. The two sides of the DHB transformer are show in Figure 7(a) and (b).

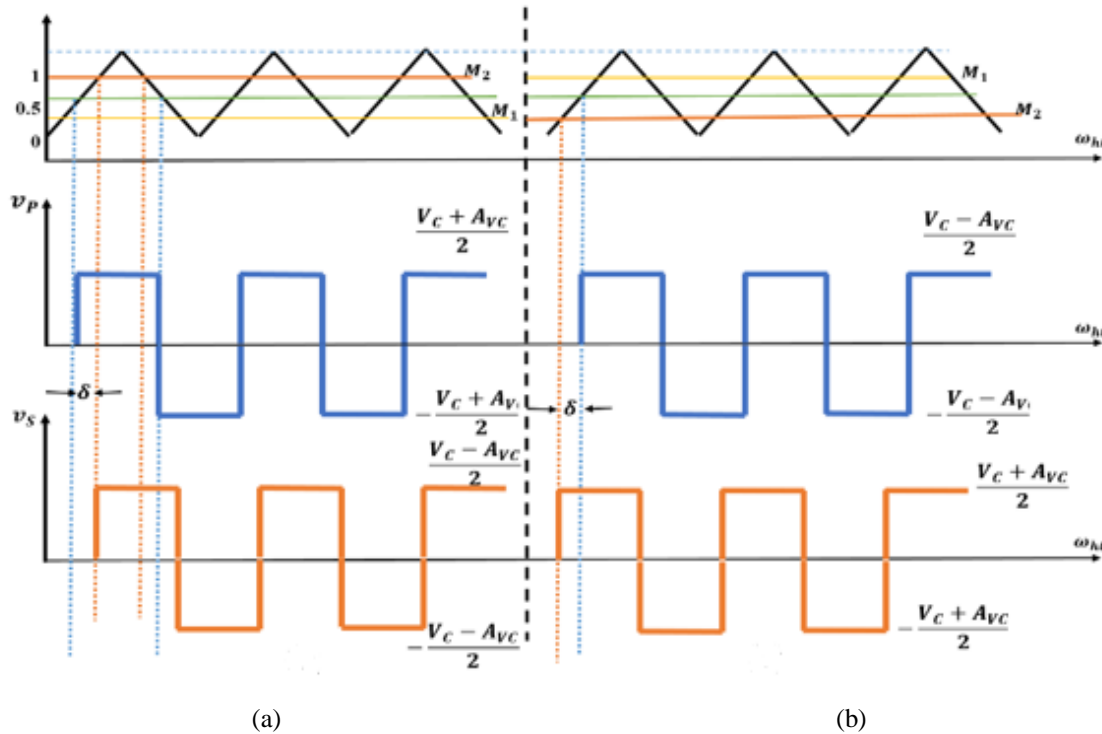(a)   (b)

Figure 7. Bi-directional power can be transmitted between both sides of the DHB transformers, (a) positive angle δ and (b) negative angle δ [21]

A carrier signal is compared to the DHB control modulator created signals M_1, M_2 to generate a DHB switching signal (S_P and S_S), produces square wave voltages on every side of the DHB module, displaced by the necessary angle δ as stated in (23) and (24).

$$M_1 = D - \frac{\delta}{\pi} \tag{23}$$

$$M_2 = |1 - M_1| \tag{24}$$

The upper of two adjacent sub-model capacitors at two phases, such as SM capacitor voltages of phase A ($\sum V_{C_{AU}}$), subtracted from phase B ($\sum V_{C_{BU}}$), is the algorithm used to regulate the DHB converter. To eliminate any harmonic wave distortion, a low-pass filter (LPF) is used. For every pair of DHBs connecting the SMs of two neighboring arms, the same control loop is repeated, with six PI controllers controlling all DHB modules, as shown in Figure (8) [21].
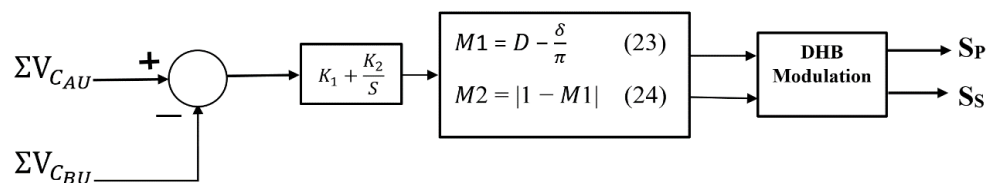

Figure 8. DHB control block diagram

3.3. The field oriented control (FOC) of induction motor

The induction motor's operating parameters are controlled using the field-oriented control (FOC) method. Figure 9 shows the schematic of the suggested MMC-DHB motor-driven system. The FOC employs two machine loop torque and flux, which are performed in the (dq) rotating frame, the FOC method uses two motor speed and flux reference values to result in the commanded torque and flux-generating elements of the stator current (i_q^* and i_d^*).

Two separate pairs of proportional-integral (PI) controllers have been utilized to process reference current components and create two groups of reference voltage vectors (V_q^* and V_d^*), which were then utilized to construct a group of three-phase reference voltages. ($V_A^*, V_B^*, and\ V_C^*$), that are applied in the MMC modulation. The control system of operation behavior of FOC is summarized in a block diagram given in Figure 9, and each step is discussed in [21].
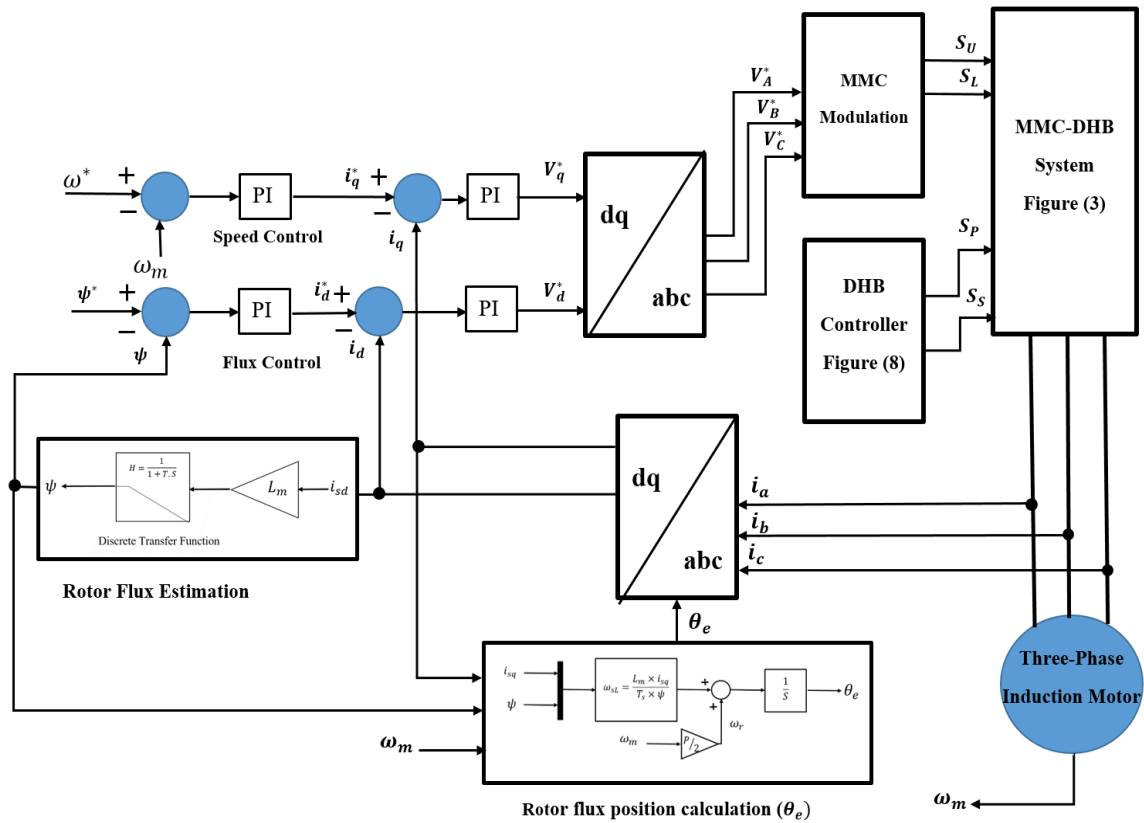

Figure 9. Schematic diagram of MMC-DHB control system

3.3.1 The Rotor Fux Block Estimation

The reference currents are used to calculate the rotor flux angle. The field-oriented control current model equations are used to determine the rotor flow vector, which necessitates a rotor speed measurement According to (25), the rotor flux estimation block is implemented as shown in Figure 10, [27]-[28].

$$\psi = \frac{L_m * i_{sd}}{1 + T_S} \qquad (25)$$

where,

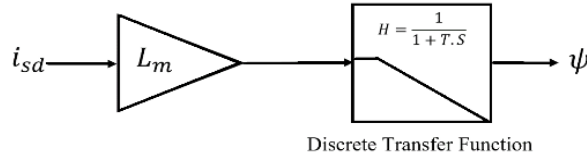$$T = \frac{R_r}{L_r}, L_r = \overline{L}_{l_r} + L_m$$

Figure 10. The rotor flux estimation block.

3.3.2. The Rotor Flux Position

The flux position may be computed in a motor model by considering terminal characteristics such as voltage and currents, but it is very sensitive to the rotor time constant. According to (26), the rotor block estimation is shown in Figure 11 [27]-[28].

$$\begin{cases} \theta_e = \int (\omega_r + \omega_{sL})dt \\ \quad \omega_r = \frac{p}{2}\omega_m \\ \quad \omega_{sL} = \frac{L_m i_{sq}}{T_s \psi} \end{cases} \tag{26}$$
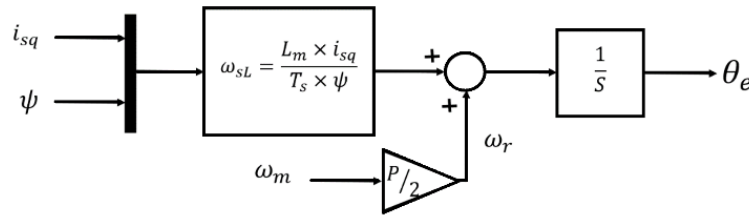

Figure 11. The rotor flux position calculation (θ_e)

4.   SYSTEM SIMULATION

The MATLAB/Simulink is used for simulation of the traditional MMC-Drive system, and the MMM-DHB drive system. The MMC-DHB is implemented in the simulation research, where each adjacent-arm SM is interfaced through a chain-link of three DHB modules, as illustrated in the previous section. Table 1 shows the parameters of the system.

Table 1. System parameters for simulation

Parameters	Values
Input DC voltage	800 V
No. of SMs in each arm	2
SM capacitor voltage Vc	400 V
Rated frequency f_o	50 Hz
PWM Carrier frequency fc	5 kHz
Arm inductance L_{arm}	2.4 m H
SM capacitance C	2 mF
DHB Parameters	
Transformer turns ratio leakage inductance	35μH
Switching frequency f_h	10 kHz
Induction Motor Parameters	
Induction Motor output Power	5.4 HP
Induction Motor Line-line Voltage	400 V
No. of Poles	4
Fundamental Frequency	50 Hz
Rated Speed nr	1430 rpm
Magnetizing Inductance L_m	0.1722 H
Stator Resistance Rs	1.405 Ω
Rotor Resistance Rr	1.395 Ω
Stator Leakage Inductance Lls	0.005839 H
Rotor Leakage Inductance Llr	0.005839 mH

5. RESULTS AND DISCUSSION

To verify the proposed conventional-MMC and MMC-DHB drive systems the MATLAB/Simulink has been used to implement a 5.4 hp ($\cong$ 4 kW), 400 V line voltage induction motor. Two separate pairs of proportional-integral (PI) controllers were used to process the reference current components and create two sets of voltage reference vectors (V_{sq}^* and V_{sd}^*). These vectors were used to create a set of three-phase reference voltages. Figure 12 shows the speed of (ωm=1430 rpm) with load torque 100% (TL=25 N ·m), which phase A chosen. The cell capacitor voltages are also well regulated within around 7 V for traditional MMC drive, as shown in Figure 12(a), and Figure 12(b), current (i_A) is sinusoidal with a fundamental frequency, 50 Hz, as illustrated in Figure 12(c). In contrast, Figure 13 shows the DHB-MMC drive equal to 2 V, at the same rated speed and current as illustrated in Figure 13(a)-(c), respectively.

In Figure 14 the machine operates at (ωm=715 rpm) with 100% load torque (TL=25 N.m). There is a clear reduction of ripple with the DHB energy-balanced system. The fluctuation of capacitor voltage decreases from (15 V$_{P-P}$) as shown in Figure 14(a), with its output current, were illustrated in Figure 14(b) to (1 V$_{P-P}$) as shown in Figure 14(c). Approximately sinusoidal output current for the DHB system is shown in Figure 14(d).
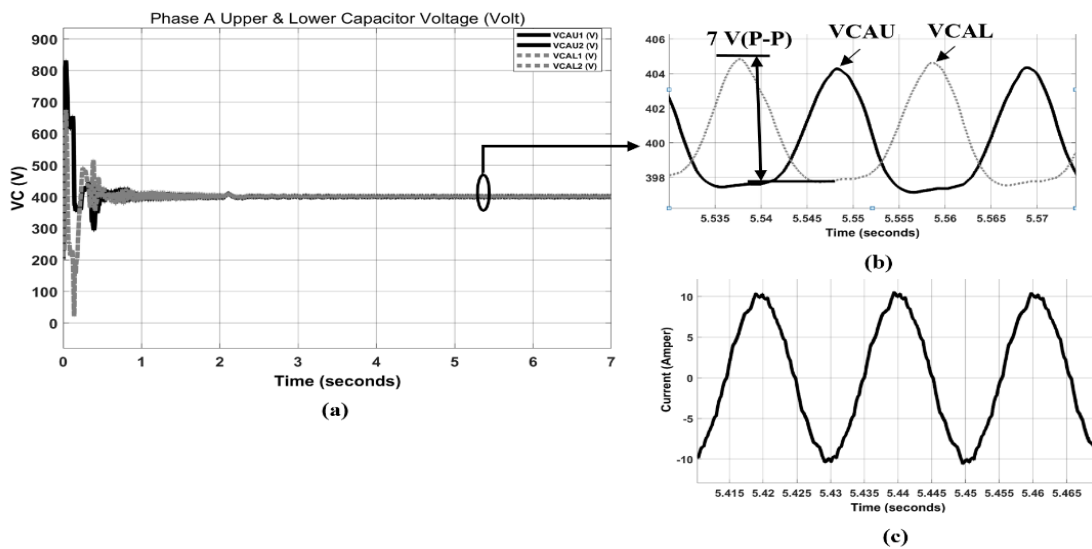

Figure 12. MMC representation at 1430 rpm where (a) represent the capacitor voltage of phase A, (b) the specific time period of the response curve, and (c) output current for traditional MMC drive system respectively
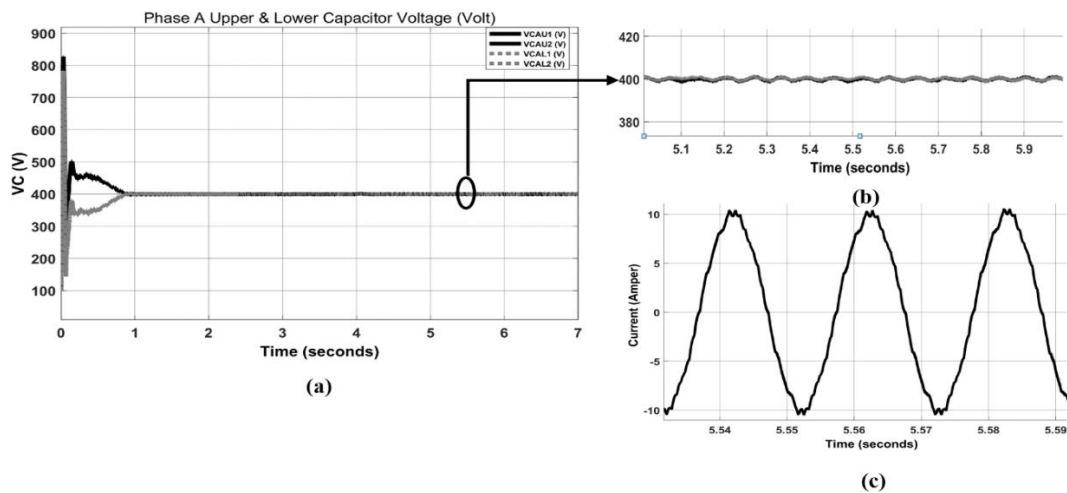

Figure 13. MMC-DHB representation at 1430 rpm where (a) represent the capacitor voltage of phase A, (b) the specific time period of the response curve, and (c) output current for the MMC-DHB drive system respectively

In Figure 15, the machine operates at (ωm=286 rpm), 100% load torque (TL=25 N.m), which offers a good indication for the capacitor voltage ripple to be reduced from (40 VP-P) as shown in Figure 15 a with its output current shown in Figure 15(b), to (1 VP-P) as shown in Figure 15(c) when the DHB is employed. Also, the output current with better shape in the MMC-DHB system is illustrated in Figure 15(d).

(a)   (b)

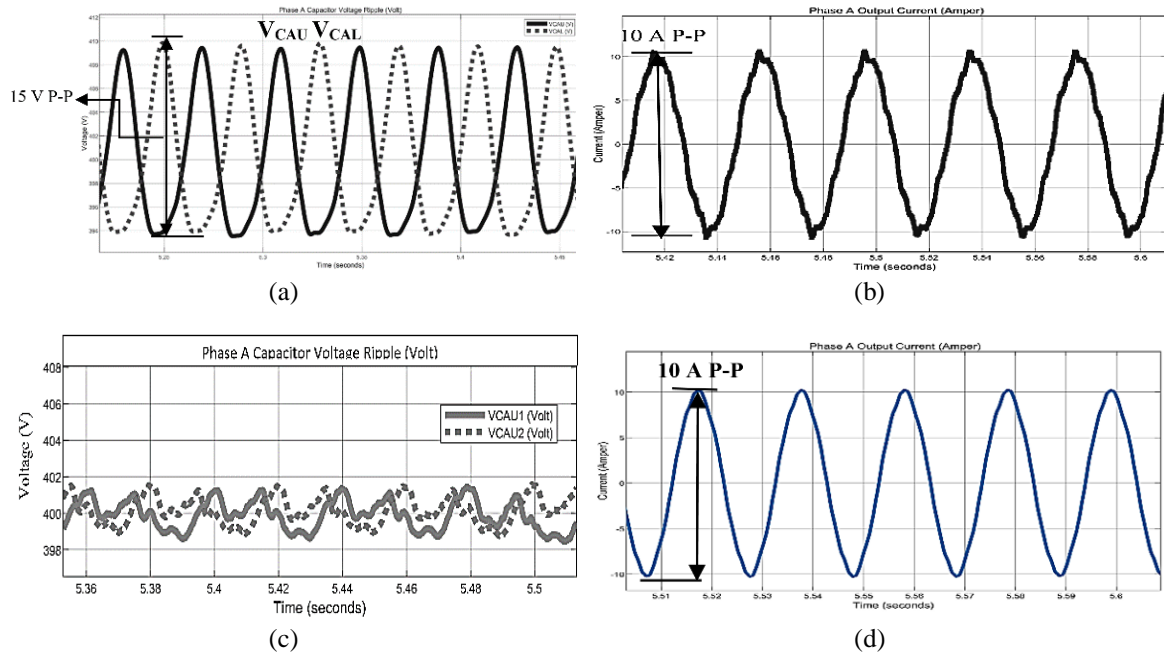(c)   (d)

Figure 14. MMC performance at 715 rpm where (a) represent the capacitor voltage, (b) the output current for traditional MMC drive system respectively, (c) represents the capacitor voltage, and (d) the output current of MMC-DHB drive system respectively

(a)   (b)
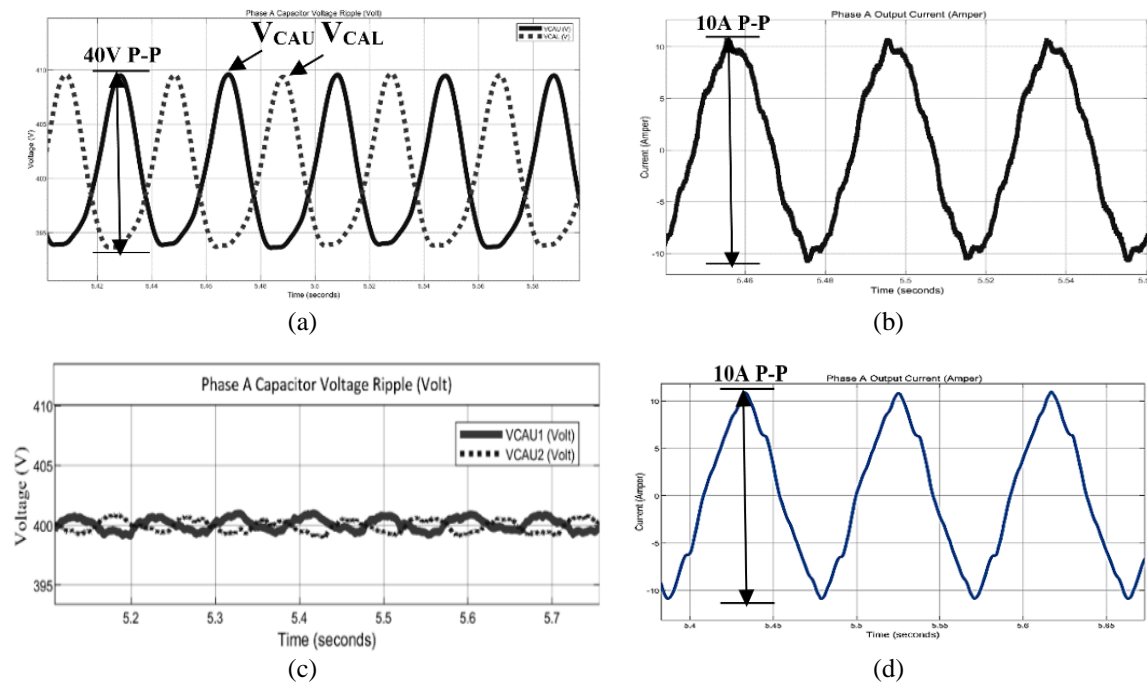
(c)   (d)

Figure 15. MMC performance at 286 rpm where (a) represent the capacitor voltage, (b) the output current for traditional MMC drive system respectively, (c) represents the capacitor voltage, and (d) the output current of MMC-DHB drive system respectively

Figure 16 shows the machine speed of 143 rpm at 100% load torque (TL=25 N.m), there is a high reduction of ripple for the DHB power balancing system, the fluctuation of capacitor voltage decreases from (50 V P-P) as shown in Figure 16(a), and its output current as shown in Figure 16(b), to (1 V P-P) as shown in Figure 16(c), and sinusoidal three-phase output currents are shown in Figure 16(d), for the MMC-DHB system compared with a traditional system.
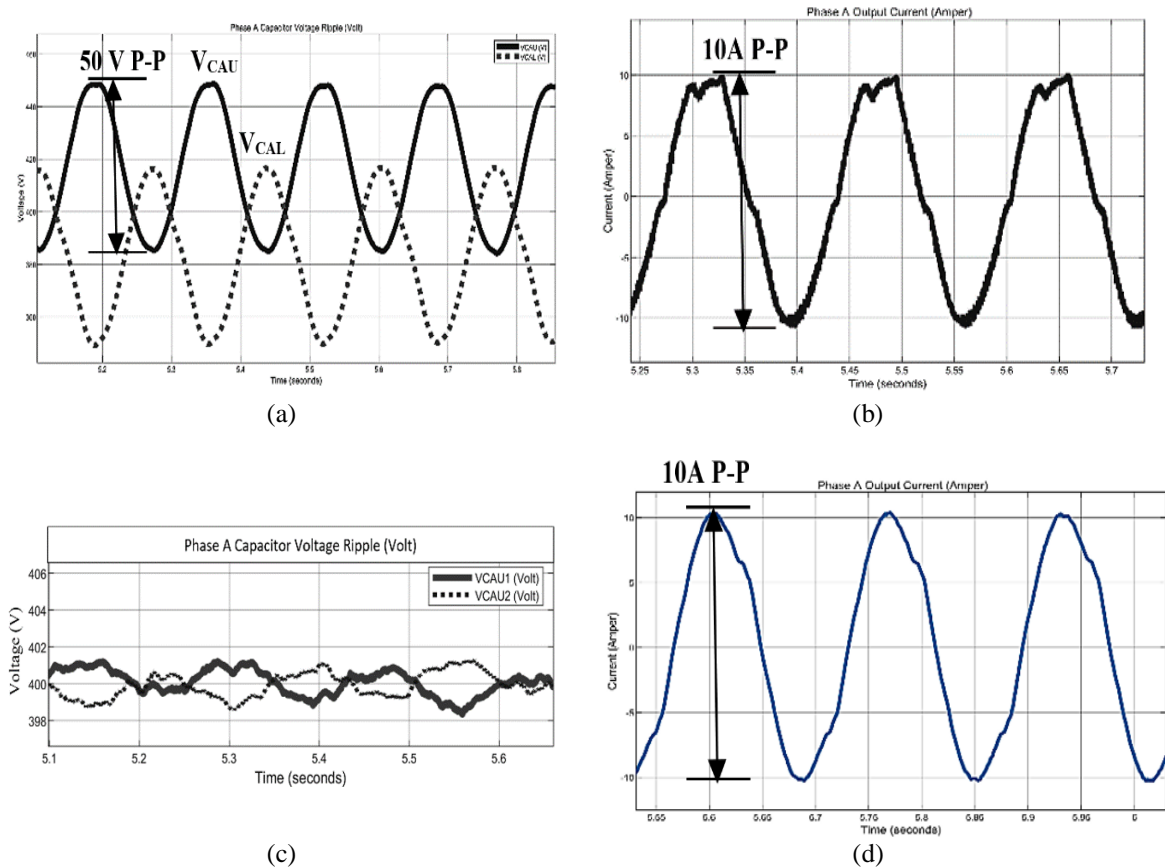

(a)

(b)

(c)

(d)

Figure 16. MMC performance at 143 rpm where (a) represent the capacitor voltage, (b) the output current for traditional MMC drive system respectively, (c) represents the capacitor voltage, and (d) the output current of MMC-DHB drive system respectively

6.   CONCLUSION

The modelling, control, and design consideration were taken in this paper for the MMC-DHB drive system with the primary emphasis on comparing with the conventional MMC drive system. The main contributions are presented in the following way: i) While the voltage ripple, regardless of the operating frequency, stays almost constant, a substantial decrease in SM capacitance is feasible. At low operating speeds, multiple megawatt machines may be driven. ii) The results showing the effective decoupling of the ripple power technique on the ripple of SM capacitor voltage reduction, at a variable frequency of operation have been obtained compared with that of the traditional MMC drive system. At 1430 rpm the capacitor voltage ripple has been reduced. from $\pm1.75\%$ to $\pm0.25\%$, the voltage ripple of the capacitor at 715 rpm decreases from $\pm3.75\%$ to $\pm0.25\%$, At lower operating frequencies, the DHB power decoupling has significant effects, as shown, the voltage ripple of a capacitor at 286 rpm decreases from $\pm10\%$ to $\pm0.25\%$, whereas the voltage ripple of the capacitor at 143 rpm decreases from $\pm12.5\%$ to $\pm0.25\%$. Instead of using a traditional-MMC drive system, a DHB-MMC-based drive system produces a high-quality sinusoidal waveform of output currents in a wide range of operating speeds.

REFERENCES

[1] J. Pou, S. Ceballos, G. Konstantinou, V. G. Agelidis, R. Picas, and J. Zaragoza, "Circulating current injection methods based on instantaneous information for the modular multilevel converter," *IEEE Transactions on Industrial Electronics*, vol. 62, no. 2, pp. 777–788, Feb. 2015, doi: 10.1109/TIE.2014.2336608.

[2] W. Liu, K. Zhang, X. Chen, and J. Xiong, "Simplified model and submodule capacitor voltage balancing of single-phase AC/AC modular multilevel converter for railway traction purpose," *IET Power Electronics*, vol. 9, no. 5, pp. 951–959, Apr. 2016, doi: 10.1049/iet-pel.2015.0120.

[3] R. Yang et al., "Asymmetric mode control of MMC to suppress capacitor voltage ripples in low-frequency, low-voltage conditions," *IEEE Transactions on Power Electronics*, vol. 32, no. 6, pp. 4219–4230, Jun. 2017, doi: 10.1109/TPEL.2016.2600762.

[4] Y. S. Kumar and G. Poddar, "Medium-voltage vector control induction motor drive at zero frequency using a modular multilevel converter," *IEEE Transactions on Industrial Electronics*, vol. 65, no. 1, pp. 125–132, Jan. 2018, doi: 10.1109/TIE.2017.2721927.

[5] M. M. Harin, V. Vanitha, and M. Jayakumar, "Comparison of PWM techniques for a three-level modular multilevel inverter," *Energy Procedia*, vol. 117, pp. 666–673, Jun. 2017, doi: 10.1016/j.egypro.2017.05.180.

[6] S. S. Lee and Y. E. Heng, "A voltage level based predictive direct power control for modular multilevel converter," *Electric Power Systems Research*, vol. 148, pp. 97–107, Jul. 2017, doi: 10.1016/j.epsr.2017.03.023.

[7] C. E. S. Feloups and E. E. M. Mohamed, "Design and Implementation of a new multilevel inverter employing reduced components," *OALib*, vol. 06, no. 09, pp. 1–17, 2019, doi: 10.4236/oalib.1105689.

[8] Z. Liu, S. Miao, Z. Fan, K. Chao, and Y. Liu, "Characteristics analysis and improved arm control of modular multilevel converter under asymmetric operation conditions," *International Journal of Electrical Power and Energy Systems*, vol. 105, pp. 272–282, Feb. 2019, doi: 10.1016/j.ijepes.2018.08.037.

[9] L. Bessegato, K. Ilves, L. Harnefors, S. Norrga, and S. Ostlund, "Control and admittance modeling of an AC/AC modular multilevel converter for railway supplies," *IEEE Transactions on Power Electronics*, vol. 35, no. 3, pp. 2411–2423, Mar. 2020, doi: 10.1109/TPEL.2019.2930321.

[10] S. Wang, D. Bao, G. Gontijo, S. Chaudhary, and R. Teodorescu, "Modeling and mitigation control of the submodule-capacitor voltage ripple of a modular multilevel converter under unbalanced grid conditions," *Energies*, vol. 14, no. 3, p. 651, Jan. 2021, doi: 10.3390/en14030651.

[11] H. Pourgharibshahi, S. Jafarishiadeh, H. Mahmoudi, H. Zargarzadeh, and R. Ahmadi, "Novel single-armed modular multilevel converter for reducing total converter capacitance," *IET Power Electronics*, vol. 14, no. 4, pp. 760–774, Mar. 2021, doi: 10.1049/pel2.12061.

[12] Y. S. Kumar and G. Poddar, "Balanced Submodule operation of modular multilevel converter-based induction motor drive for wide-speed range," *IEEE Transactions on Power Electronics*, vol. 35, no. 4, pp. 3918–3927, Apr. 2020, doi: 10.1109/TPEL.2019.2938096.

[13] M. Noushak, A. Hadizadeh, H. Iman-Eini, S. Farhangi, and D. Frey, "Reduction of capacitor voltage ripple in a modular multilevel converter employed in adjustable speed drive application," in *8th Power Electronics, Drive Systems and Technologies Conference, PEDSTC 2017*, 2017, pp. 317–322, doi: 10.1109/PEDSTC.2017.7910345.

[14] H. R. Parikh, R. S. M. Loeches, G. Tsolaridis, R. Teodorescu, L. Mathe, and S. Chaudhary, "Capacitor voltage ripple reduction and arm energy balancing in MMC-HVDC," in *EEEIC 2016 - International Conference on Environment and Electrical Engineering*, Jun. 2016, pp. 1–6, doi: 10.1109/EEEIC.2016.7555778.

[15] J. Kolb, F. Kammerer, M. Gommeringer, and M. Braun, "Cascaded control system of the modular multilevel converter for feeding variable-speed drives," *IEEE Transactions on Power Electronics*, vol. 30, no. 1, pp. 349–357, Jan. 2015, doi: 10.1109/TPEL.2014.2299894.

[16] S. Sau and B. G. Fernandes, "Modular multilevel converter based variable speed drives with constant capacitor ripple voltage for wide speed range," in *Proceedings IECON 2017 - 43rd Annual Conference of the IEEE Industrial Electronics Society*, Oct. 2017, vol. 2017-January, pp. 2073–2078, doi: 10.1109/IECON.2017.8216348.

[17] B. Li, S. Zhou, D. Xu, S. J. Finney, and B. W. Williams, "A hybrid modular multilevel converter for medium-voltage variable-speed motor drives," *IEEE Transactions on Power Electronics*, vol. 32, no. 6, pp. 4619–4630, Jun. 2017, doi: 10.1109/TPEL.2016.2598286.

[18] M. Saeedifard and R. Iravani, "Dynamic performance of a modular multilevel back-to-back HVDC system," *IEEE Transactions on Power Delivery,* vol. 25, no. 4, pp. 2903–2912, Oct. 2010, doi: 10.1109/TPWRD.2010.2050787.

[19] B. M. Espinoza, A. Mora, M. Diaz, and R. Cárdenas, "Balancing energy and low-frequency operation of the modular multilevel converter in back to back configuration," *in 2015 10th International Conference on Ecological Vehicles and Renewable Energies, EVER 2015,* Mar. 2015, pp. 1–9, doi: 10.1109/EVER.2015.7113005.

[20] B. Li, S. Zhou, L. Han, J. Wang, and D. Xu, "Back-to-back modular multilevel converter topology with DC-link switches for high-power four-quadrant variable speed motor drives," in *2019 21st European Conference on Power Electronics and Applications, EPE 2019 ECCE Europe*, Sep. 2019, p. P.1-P.7, doi: 10.23919/EPE.2019.8914791.

[21] M. S. Diab, A. M. Massoud, S. Ahmed, and B. W. Williams, "A modular multilevel converter with ripple-power decoupling channels for three-phase MV adjustable-speed drives," *IEEE Transactions on Power Electronics*, vol. 34, no. 5, pp. 4048–4063, May 2019, doi: 10.1109/TPEL.2018.2858003.

[22] M. S. Diab, A. M. Massoud, S. Ahmed, and B. W. Williams, "A Dual modular multilevel converter with high-frequency magnetic links between submodules for MV open-end stator winding machine drives," *IEEE Transactions on Power Electronics*, vol. 33, no. 6, pp. 5142–5159, Jun. 2018, doi: 10.1109/TPEL.2017.2735195.

[23] M. S. Diab, B. W. Williams, D. Holliday, A. M. Massoud, and S. Ahmed, "A modular multilevel converter with isolated energy-balancing modules for MV drives incorporating symmetrical six-phase machines," *in 2017 IEEE Energy Conversion Congress and Exposition, ECCE 2017,* Oct. 2017, vol. 2017-January, pp. 2715–2722, doi: 10.1109/ECCE.2017.8096509.

[24] B. Li, R. Yang, D. Xu, G. Wang, W. Wang, D. Xu," Analysis of the phase-shifted carrier modulation for modular multilevel converters," *IEEE Transactions on Power Electronics*, vol. 30, no. 1, January 2015, doi: 10.1109/TPEL.2014.2299802.

[25] M. Abdelsalam, M. Marei, S. Tennakoon, and A. Griffiths, "Capacitor voltage balancing strategy based on sub-module capacitor voltage estimation for modular multilevel converters," *CSEE* Journal of Power and Energy Systems, vol. 2, no. 1, pp. 65–73, Mar. 2016, doi: 10.17775/cseejpes.2016.00010.

[26] M. Hagiwara and H. Akagi, "Control and experiment of pulse-width-modulated modular multilevel converters," *IEEE Transactions on Power Electronics*, vol. 24, no. 7, pp. 1737–1746, Jul. 2009, doi: 10.1109/TPEL.2009.2014236.

[27] Y. Li and L. Fan, "Modular multilevel converter based induction machine drive," in *2015 North American Power Symposium, NAPS 2015*, Oct. 2015, pp. 1–6, doi: 10.1109/NAPS.2015.7335129.

[28]   H. U. Haq, M. H. Imran, H. I. Okumuş, and M. Habibullah, "Speed control of induction motor using FOC method," *International Journal of Engineering Research and Applications*, vol. 5, no. 3, pp. 154–158, 2015.

BIOGRAPHIES OF AUTHORS

Eaam Abdul-Khaliq Ali ⓘ SC 🔍 Ⓟ Received the B.Sc. degree in electrical engineering from Mustansiriyah University, the M.Sc. degree in electrical engineering from the University of Baghdad, Power Electronics Specialization. She holds a PhD degree in electrical engineering, Power Electronics Specialization from Baghdad University. Her research area is the reduction of capacitor voltage ripple in modular multilevel converter using power decoupling channel. She was a lecturer for (power electronics, power system, power distribution system) subjects in the Electrical Engineering Department/College of Engineering/Mustansiriyah University. She can be contacted at email: enaamalimsc2009@yahoo.com, Enaamali2018@uomustansiriyah.edu.iq

Prof. Dr Turki Kahawish Hassan ⓘ 🔍 SC Ⓟ He has received B.Sc. in Electrical Engineering in 1982, M.Sc. in Electrical Engineering/Power Electronics Specialization in 1991, and a PhD in Electrical Engineering/Power Electronics Specialization in 2005 from Iraq/University of Baghdad/College of Engineering/Electrical Engineering Department. From 1983–to 2005 he worked in Electrical Engineering Design Centre as a designer for DC-AC converters and AC-DC converters. From 2006 up to now He was a lecturer for power electronics subject in the Electrical Engineering Department /College of Engineering/Mustansiriyah University. He was a professor in 2020. His research interests include modular multilevel converters, high-frequency DC-DC converters, AC Drive Systems, and Grid-Connected Photovoltaic Systems. He has published 27 journal articles and 5 international conference articles. He can be contacted at email: Turki_k.eng@uomustansiriyah.edu.iq.